

Progress towards intersubband quantum-box lasers for highly efficient continuous wave operation in the mid-infrared

Dan Botez,^a Gene Tsvid,^a Mithun D'Souza,^a Manish Rathi,^a Jae C. Shin,^a Jeremy Kirch,^a Luke J. Mawst,^a Thomas Kuech,^a Igor Vurgaftman,^b Jerry Meyer,^b Jason Plant,^c and George Turner^c

^a Reed Center for Photonics, University of Wisconsin, 1415 Engineering Drive, Madison, WI 53706

botez@engr.wisc.edu

^b Code 5613, Naval Research Laboratory, Washington, DC 20375

^c MIT Lincoln Lab MS: C215, 244 Wood St., Lexington, MA 02420

Abstract. Intersubband quantum-box (IQB) lasers, which are devices consisting of 2-D arrays of ministacks (i.e., 2-4 stages) intersubband QB emitters have been proposed as alternatives to 30-stage quantum-cascade (QC) devices, for efficient room-temperature (RT) emission in the mid-infrared (4-6 μm) wavelength range. Preliminary results include: 1) the design of devices for operation with 50% wallplug efficiency at RT; 2) realization of a novel type of QC device: the deep-well (DW) QC laser, that has demonstrated at $\lambda = 4.7 \mu\text{m}$ low temperature sensitivity of the threshold current, a clear indication of suppressed carrier leakage; 3) the formation of 2-D arrays at nanopoles by employing nanopatterning and dry etching; 4) the formation of 40 nm-diameter, one-stage IQB structures on 100 nm centers by preferential regrowth via metal-organic vapor phase epitaxy (MOVPE).

Keywords: Intersubband-transition semiconductor laser, quantum boxes, phonon bottleneck.

1 INTRODUCTION

Semiconductor lasers operating in continuous wave (CW) at or near room temperature (RT) and emitting in the mid- and far-infrared wavelength ranges: 3-13 μm ; are critically needed for a vast array of applications. Intersubband (IS) transition emitters are the most likely solution. The first implementation of the concept for using IS transitions for laser action [1], was realized in early 1994 [2] and named quantum cascade (QC) laser. Current QC devices have demonstrated high-power, RT CW operation in the 4.0-6.0 μm range [3,4], but with relatively low wallplug efficiency ($\sim 9\%$) due to inherently high voltages (10-11V). Furthermore, the devices have extremely temperature-sensitive characteristics [3-5] at and above RT, due to thermionic carrier leakage, which in turn raises serious issues of long-term device reliability.

Quantum-well (QW) lasers involving IS transitions have fundamentally poor radiative efficiencies since the nonradiative, LO-phonon-assisted relaxation time for electrons in the upper laser states is about 1.8 ps [6], whereas the radiative relaxation time is 4.2 ns. That is, nonradiative processes are about 2300 times faster than radiative processes. Since there are good reasons to believe that the LO-phonon-assisted relaxation time will substantially increase if the relaxing electrons are confined in quantum boxes [7-16], the radiative efficiency problem can be overcome by replacing the QW active regions of a QC laser with a quantum-box (QB) 2-D array [17] or a 2-D array of cascaded QBs [18].

2 IQB LASERS: DESIGN AND PROJECTED PERFORMANCE

In QW structures the relaxation between subbands occurs [2,6] in about 2 ps, primarily via LO-phonon absorption or emission [6,7]. Making quantum boxes (QBs) causes discrete states in the subbands [17] which in turn causes the LO-phonon-assisted electron relaxation time to increase [7,9] by a factor β [17]. This is the so called phonon bottleneck. Experimental results [10-14] from QBs and photocurrent-response/dark-current measurements from QB IR detectors [11,15] indicate electron-relaxation times of the order of 100 ps, in good agreement with theory [16]. As the temperature increases to RT the relaxation times decrease [12,13] due to the inherent carrier loss, in self-assembled QBs, to wetting layers [19]. The proposed QBs are not self-assembled and thus can be made *deep* (i.e., negligible carrier leakage with increasing temperature). Thus, for deep InGaAs/GaAs QBs β may well be as high as 50 at RT.

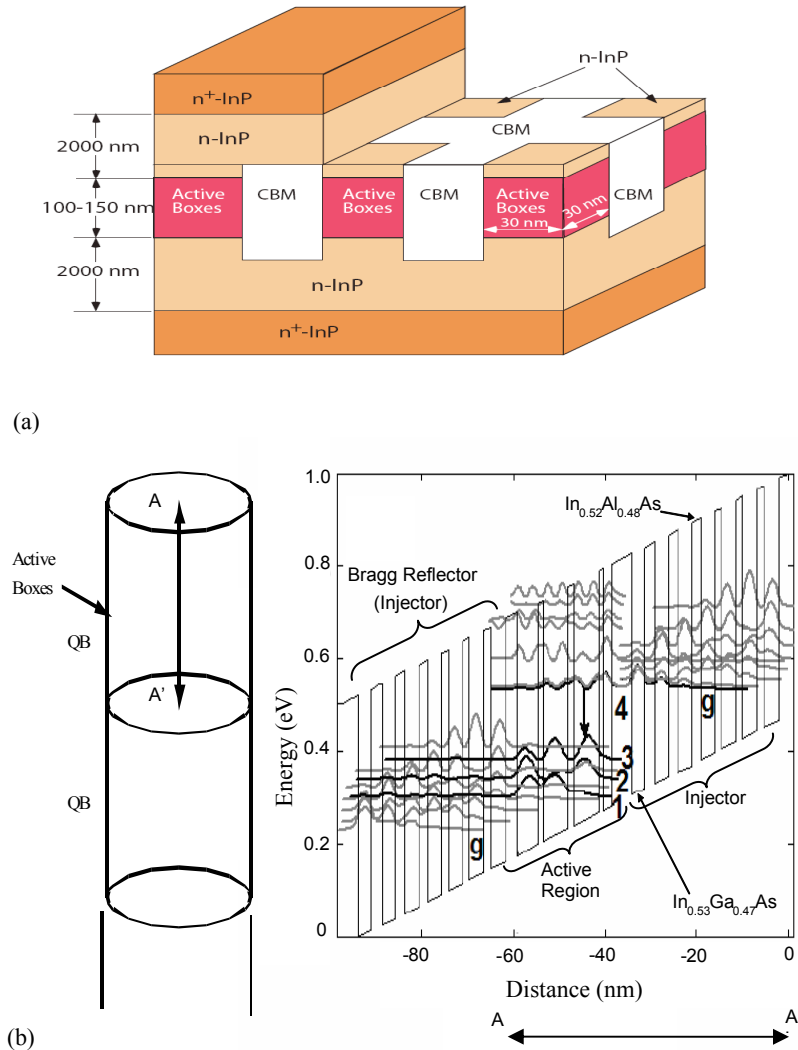


Fig. 1. (a) Representation of the IQB structure (CBM=Current Blocking Material), (b) Schematic representation of a QB ministack (i.e., active boxes) and the conduction-band energy diagram inside one QB, indicated by the AA' line, which is like one stage in a QC structure.

The proposed device is schematically shown in Fig. 1: an IS-transition laser with an active region composed of a 2D array of QB ministacks, called "active boxes," separated by current-blocking material. Each ministack is composed of 2 to 4 QBs, sequentially arranged like the stages in a QC-laser structure. The ministacks of QBs are fabricated by dry etching and regrowth, allowing for tight carrier confinement *unlike* the inherently weak carrier confinement of self-assembled QBs. The active-boxes array together with low-doped, n-type InP layers constitute the core of an optical waveguide with heavily doped n-type InP cladding layers. The active region is designed to have deep wells in energy [20] (not shown), which, due to the high energy barrier for electrons in the upper energy state E_4 (i.e., $\sim 400\text{meV}$), insure suppression of thermionic carrier leakage.

A 2-D array of 4-QB stacks is considered. A transverse waveguide of low loss coefficient, α_w , of 1.5 cm^{-1} has been designed. Then, for 0.75 mm-long, $20\text{ }\mu\text{m}$ -aperture devices with 10% and 90% front- and back-facet reflectivities and taking $\beta = 50$, the calculated CW wallplug efficiency, η_p , at RT reaches a maximum of 50% (Fig. 2) at $\sim 15 \times$ threshold. The J_{th} value is $\sim 0.1\text{ kA/cm}^2$, while the voltage is $< 1.7\text{ V}$, in sharp contrast to typical QC-device voltages (i.e., 11-12 V).

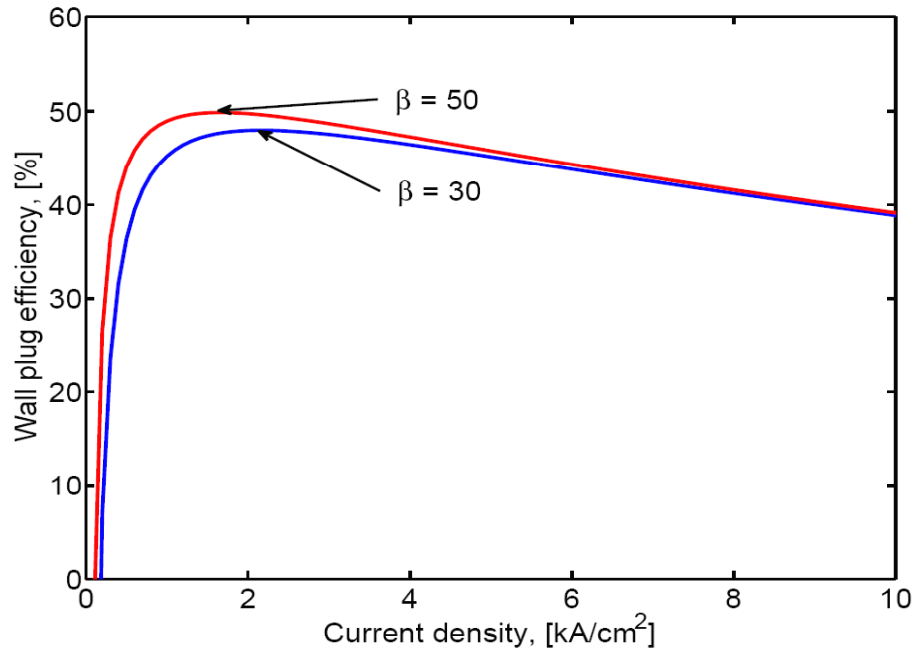


Fig. 2. Calculated RT CW wallplug efficiency vs current density for 4QB-stack devices at different β values.

We note that the use of *self-assembled* QBs in QC-like structures has been proposed [18, 21] and demonstrated [22]. RT J_{th} values as low as 10 A/cm^2 have been predicted [18] for 10-stage devices. Intersubband luminescence was observed [22] at $\lambda = 22\text{ }\mu\text{m}$, but represented only 0.8% of the total luminescence, due most probably to the inherent problem of self-assembled QBs: carrier transitions involving the wetting layers. The proposed QBs do not involve self-assembly, but actual fabrication [23], thus allowing to tightly confine the carriers

to the QBs. Due to the deep-QW proposed design carrier leakage will be suppressed as already experimentally demonstrated for single-stage QW devices [24]. Thus truly deep QBs could be realized for the first time, which in turn will allow for temperature-insensitive characteristics and subsequent high wallplug efficiencies *and* long-term device reliability.

3 PRELIMINARY RESULTS

3.1 Deep-well 4.8 μm QC lasers

The active medium of conventional QC lasers is composed of a superlattice of quantum wells and barriers of the same composition, respectively. As a result, for devices emitting in the 4.5-5.5 μm range there is substantial thermionic carrier leakage from the upper laser level to the continuum as evidenced by a strong decrease in the slope efficiency above RT (e.g., the slope-efficiency characteristic-temperature coefficient, T_1 , has a low value of ~ 130 K [4,5]) and the threshold current has low T_0 values : ~ 140 K above RT [4,25] which is understandable given the relatively small (i.e., 200 meV) energy differential, δE , between the upper lasing level and the top of the exit barrier. Thus, even though such buried-heterostructure devices show relatively high wallplug efficiency (i.e., $\sim 9\%$), the strong temperature sensitivity of their electro-optical characteristics doesn't allow for optimal performance.

To solve this problem we have designed and fabricated a QC device (Fig.3) for which carrier leakage is suppressed due to *deep* wells and tall barriers in each active region [20]. An 8-band $\mathbf{k}\cdot\mathbf{p}$ code was used. For our deep-well design δE has a value of ~ 400 meV, and thus the carrier-leakage current, which is roughly proportional to $\exp(-\delta E/kT)$, is suppressed. Another advantage of the proposed deep-well design is that the highly strained layers are located only in a portion of each stage, thereby reducing the overall strain within each stage.

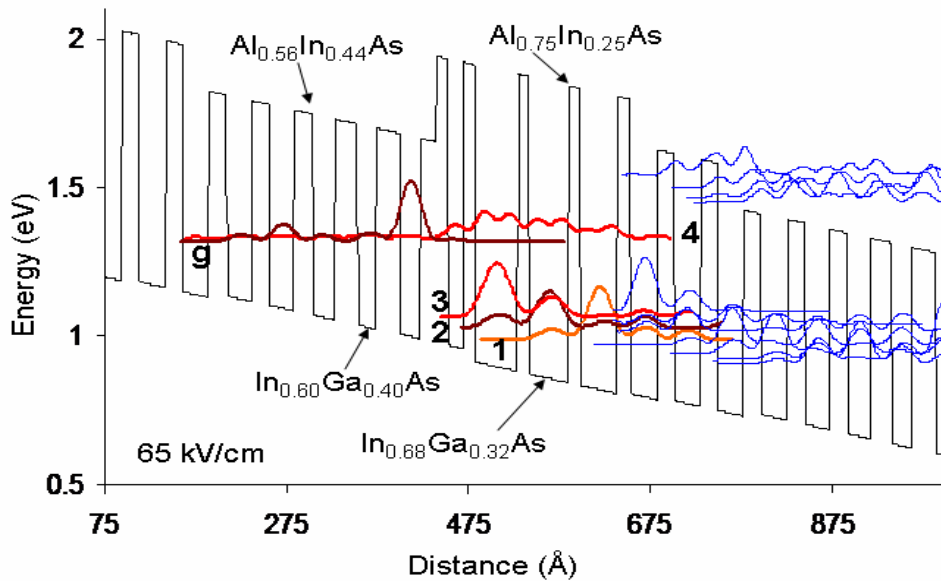


Fig. 3. Conduction band diagram and the associated wavefunctions for the deep-well, tall-barrier QC-laser design at 70 kV/cm, with a calculated emission wavelength of 4.7 μm .

A deep-well QC laser structure has been grown by MOCVD and fabricated into 19 μm -wide mesas and 3 mm-long chips. The devices lase at 4.6 μm or 4.8 μm (Fig.4) with pulsed

threshold-current densities as low as 1.5 kA/cm^2 , a value comparable to state-of-the-art $4.6\text{-}4.8 \text{ }\mu\text{m}$ conventional QC devices of same cavity length (and uncoated facets) [4] even though the matrix-element squared, $[z_{43}]^2$, is only 66% of the value for conventional $4.6\text{-}4.8 \text{ }\mu\text{m}$ QC lasers. Preliminary tests give T_0 values of 218 K over the 250-340 K temperature range (Fig. 5), for $4.65 \text{ }\mu\text{m}$ devices, compared to $\sim 140 \text{ K}$ values for conventional $4.6 \text{ }\mu\text{m}$ QC lasers over the same temperature range [4,25]. This is clear indication that carrier leakage has been substantially suppressed. For IQB devices deep wells are important since the carrier relaxation

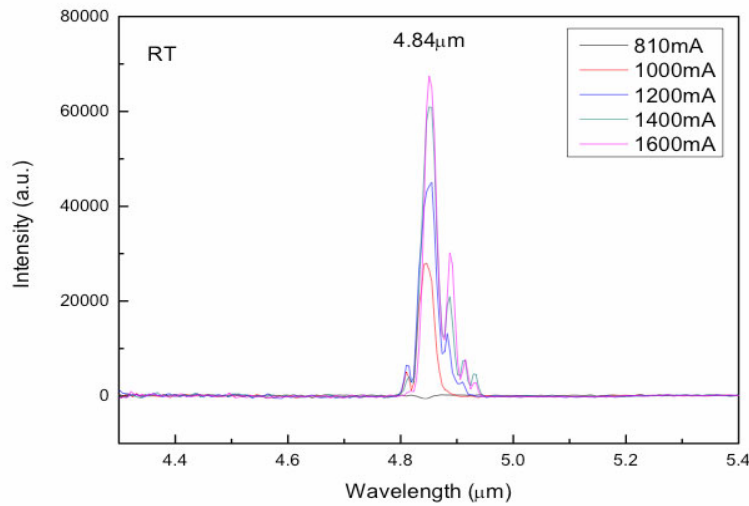


Fig.4. Spectra of a deep-well QC laser at room temperature.

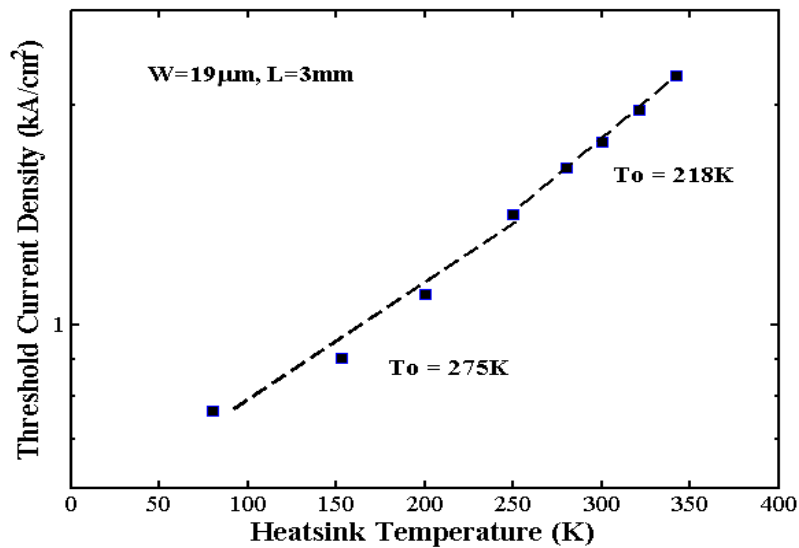


Fig. 5. Threshold-current density, J_{th} , variation as a function of heatsink temperature. T_0 is the characteristic-temperature coefficient of J_{th} . [i.e., $J_{th}(T+\Delta T) = J_{th}(T) \exp(\Delta T/T_0)$].

time is increased by a factor of 30 to 50 times compared to conventional QC devices, and thus thermionic carrier leakage out of the active wells could severely impact the device efficiency. Therefore suppression of carrier leakage is vital to the proper operation of IQB devices.

3.2 IQB Device Fabrication

3.2.1 Basic Fabrication Sequence

The basic fabrication for the realization of a 2-D QB array is schematically shown in Fig. 6. After initial MOVPE growth, the wafer is covered with a thin ($\sim 40\text{nm}$) dielectric film (e.g., SiO_2) and, after an e-beam resist is deposited, the QB-pattern is defined with a 20 nm electron beam from a e-beam lithography machine. Then RIE is used to transfer the pattern into the dielectric layer (Unlike what is shown in Fig. 6 the mask is made of disks rather than squares). The 2-D array of dielectric disks is then used as a mask for QB-stack formation. Dry etching is used to remove material (see next subsection) followed by preferential regrowth of semi-insulating InP in an MOVPE system. After the regrowth the dielectric disks are chemically removed and regrowth is performed via MOVPE to complete the structure shown in Fig. 1a.

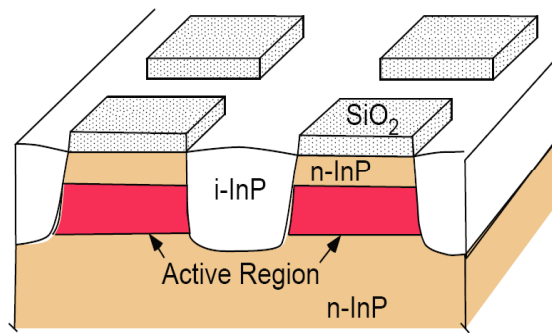


Fig. 6. Schematic representation of the fabrication for the quantum-box array.

3.2.2 Interface Passivation

For unipolar intersubband devices such as QC lasers one need *not* be concerned about loss of carriers to defects at exposed surfaces, since the transition energies involved are much smaller than the energy between midgap and the conduction-band edge at those exposed surfaces. QC lasers with exposed-surface, $10\ \mu\text{m}$ -wide ridges operate quite well. However, for nanostructures with in-plane dimensions of $\leq 50\text{nm}$ the defect density needs to be drastically reduced at the device edges, since Fermi-level pinning would cause full depletion across the devices [26]. Therefore, our QB formation was done such that virtually no charge-trapping states are formed at the QB edges, thus eliminating Fermi-level pinning.

We have carried out experiments on (110)-oriented InGaAs surfaces [27], that is, on crystalline planes equivalent to the side edge(s) of the QBs to be formed. Initially, a thick n-type InGaAs was grown on top of an n-type (110)-oriented InP wafer.

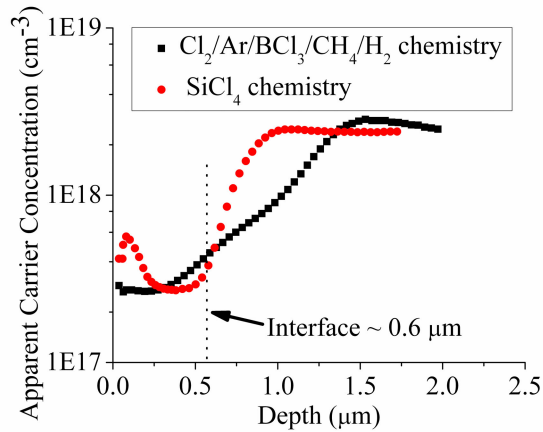


Fig. 7. ECV data for $\text{CH}_4/\text{H}_2/\text{Ar}/\text{Cl}_2/\text{BCl}_3$ and $\text{Cl}_2/\text{SiCl}_4/\text{Ar}$ plasma etching. $N_i < 10^{10}/\text{cm}^2$.

Subsequently, it was exposed to RIE etching in either a $\text{CH}_4/\text{H}_2/\text{Ar}/\text{Cl}_2/\text{BCl}_3$ or a $\text{Cl}_2/\text{SiCl}_4/\text{Ar}$ gas mixture which have been used to fabricate nanoposts for the IQB structures (see next subsection). After an annealing step and surface treatment with tartaric acid, regrowth of n-type InGaAs was carried out in an MOVPE reactor. Then electrochemical capacitance-voltage (ECV) measurements were performed on the samples to verify the doping profile and to determine the existence of trapped charges due to surface states at the interface. As evident from Fig. 7 the apparent carrier concentration vs. depth curves show no abrupt features at and around the interface, which is clear indication that the interfacial defect density, N_i , is below $10^{10}/\text{cm}^2$. In turn, that means that Fermi-level pinning has been eliminated at the interface.

3.2.3 Nanopatterning and Etching of Nanopoles

The eventual design involves a QB array of 30nm-diameter boxes of 60 nm centers (Fig. 1a), a nontrivial task. Therefore, the patterning has to be done in progressive steps. We used e-beam direct writing employing the novel resist: hydrogen silsesquioxane (HSQ); which was found best for generating high-quality, 2-dimensional dot patterns [23]: 33 nm-diameter dots on 80 nm centers. Then we transferred such patterns into Si_3N_4 , the dielectric found suitable as a mask for dry etching and regrowth.

Using 40 nm-thick Si_3N_4 disks, plasma etching was performed with both Electron Cyclotron Resonance (ECR) etching using $\text{CH}_4/\text{H}_2 + \text{Argon} + \text{BCl}_3$ as well as Inductive Coupled Plasma (ICP) etching using SiCl_4 . Using both methods we were able to obtain 30-40 nm-diameter nanopoles on spacings as low as 100nm and of a height of ~ 70 nm. This is for a 1-stage ministack device. A typical result from an ICP-etched sample is shown in Fig. 8 (The leftover Si_3N_4 regions appear as "white" caps atop the nanopoles).

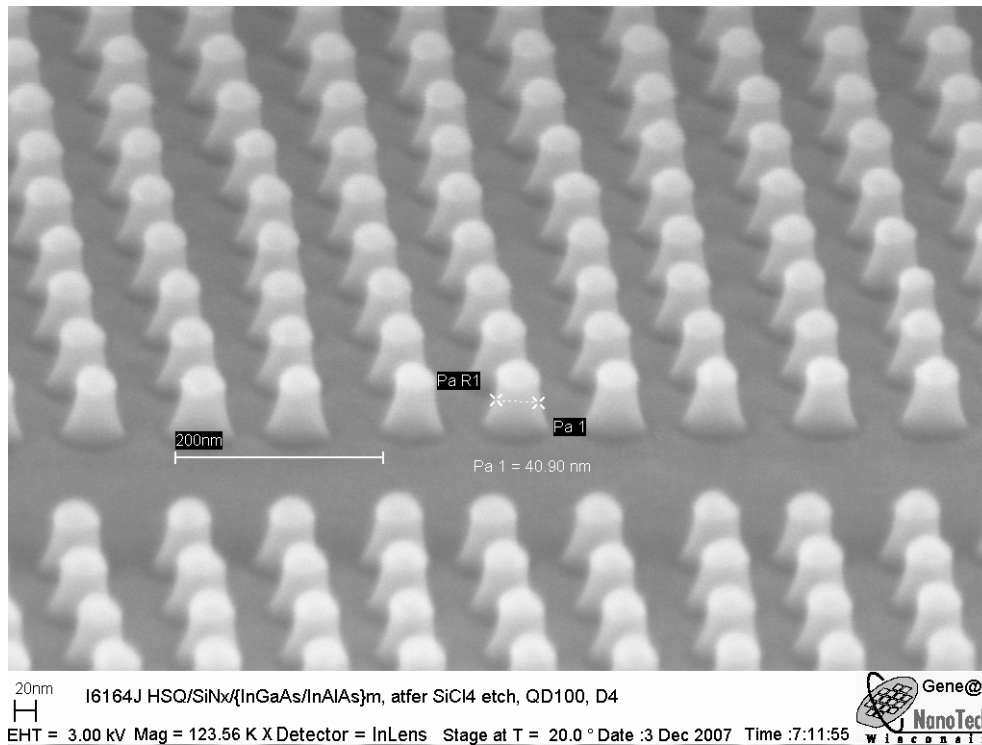
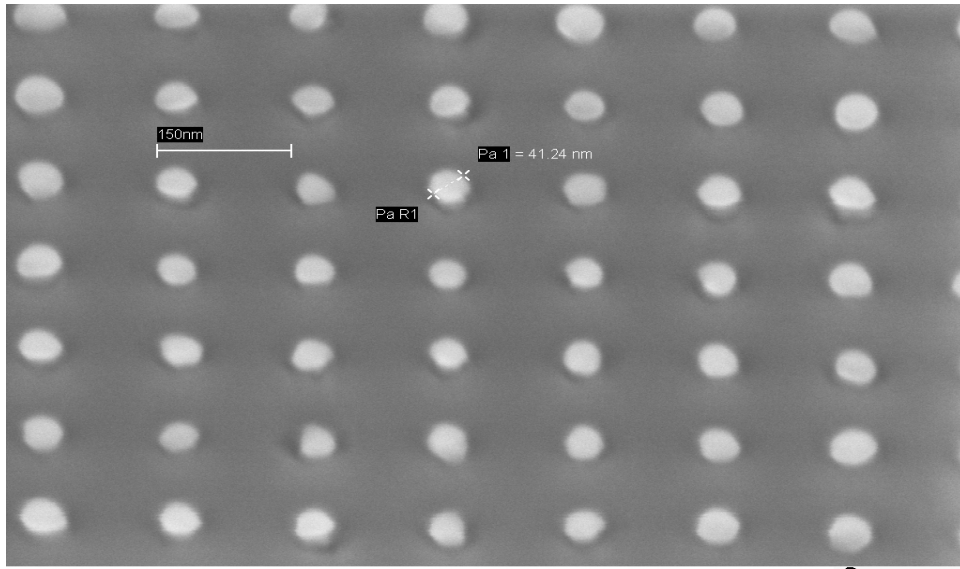


Fig. 8. Nanopoies dry etched using ICP with SiCl_4 . 40nm-diameters nanopoies are obtained on 100nm centers. The mask for etching was a 2-D array of Si_3N_4 disks.

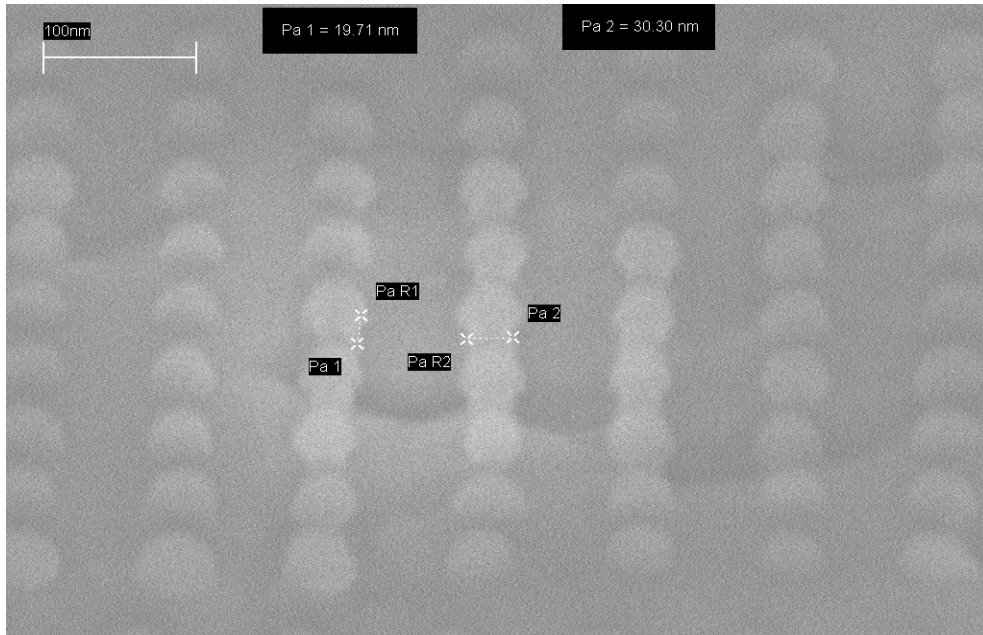
3.2.4 Regrowths for Electrical Insulation between Nanopoies

Using dry-etched nanopoies as shown in Fig. 8, we performed regrowths of semi-insulating InP to insure electrical isolation between the QBs in the nanopoies. The regrowths consisted of a thin layer of n-InGaAs followed by high-resistivity Fe-doped InP. Typical results of successful regrowths are shown in Fig. 9.

From close inspection of the SEMs we find that the top diameters of the nanopoies are in the 27-30 nm range, which in turn provides an ~ 40 nm diameter at the active region. Such results have been obtained for nanopoies on 100 nm, 125 nm and 150 nm centers. The leftover Si_3N_4 caps have been removed with HF and the rest of the regrowths for the formation of IQB-laser structures (see Fig. 1a) have been performed. Devices are in processing.



20nm I6389F, after regr 022908-1, QB150, D4
 EHT = 3.00 kV Mag = 109.49 K X Detector = InLens Stage at T = 0.0 ° Date :1 Mar 2008 Time :10:48:49



20nm I6700B after regrowth1, chip (1,3), dev 3, QB100, D1
 EHT = 10.00 kV Mag = 566.74 K X Detector = InLens Stage at T = 20.0 ° Date :7 Aug 2008 Time :17:20:09



Fig. 9. SEM images of nanopoles embedded in regrowth. Top: Top view. Bottom : Grazing-angle view.

4 CONCLUSIONS

Significant suppression of phonon-assisted electron relaxation times in deep, unipolar quantum boxes (QBs) will allow the fabrication of intersubband lasers emitting CW at room temperature in the 4-6 μm wavelength range with high (> 40%) wallplug efficiency. Since the backfilling effect characteristic of cascaded QW lasers is a moot issue and thermionic carrier leakage will be suppressed via the use of deep active wells, IQB lasers are unlikely to suffer from the thermal runaway that currently mars the performance of CW QC lasers and thus should prove to be highly reliable devices. Preliminary results include the first demonstration of deep-well QC lasers which, as expected, have threshold currents much less sensitive to temperature than those of conventional QC lasers, the development of a passivation technique that eliminates trapped-charge defects at interfaces corresponding to the QB's sidewalls, the patterning and dry etching of 30-40nm-diameter nanopoles on center-to-center spacings as small as 100nm, and the successful regrowth of semiinsulating material around the nanopoles.

Acknowledgments

This material is based on research sponsored by DARPA under agreement number FA8650-07-1-7709. The U.S. government is authorized to reproduce and distribute reprints for Governmental purposes notwithstanding any copyright notation thereon. The authors are grateful for valuable technical discussions with Claire Gmachl and Peter Zory.

References

- [1] R. F. Kazarinov and R. A. Suris, "Possibility of the amplification of electromagnetic waves in a semiconductor with a superlattice," *Sov. Phys. Semicond.* **5**, 707-709 (1971).
- [2] J. Faist, F. Capasso, D. L. Sivco, C. Sirtori, A. L. Hutchinson, and A. Y. Cho, "Quantum cascade laser," *Science* **264**, 553-556 (1994) [doi:10.1126/science.264.5158.553].
- [3] A. Evans, S. R. Darvish, S. Slivken, J. Nguyen, Y. Bai, and M. Razeghi, "Buried heterostructure quantum-cascade lasers with high continuous wave wallplug efficiency," *Appl. Phys. Lett.* **91**, 071101(2007) [doi:10.1063/1.2770768].
- [4] A. Lyakh, C. Pflugl, L. Diehl, Q. J. Wang, F. Capasso, X. J. Wang, J. Y. Fan, T. Tanbuk-Ek, R. Maulini, A. Tsekoun, R. Go, and C. K. N. Patel, "1.6W high wallplug efficiency, continuous-wave, room temperature quantum cascade laser emitting at 4.6 μm ," *Appl. Phys. Lett.* **92**, 111110 (2008) [doi:10.1063/1.2899630].
- [5] J. S. Yu, S. Slivken, A. J. Evans, and M. Razeghi, "High performance continuous-wave operation of $\lambda \sim 4.6 \mu\text{m}$ quantum-cascade lasers above room temperature," *IEEE J. Quantum Electron.* **44**, 747-754 (2008) [doi:10.1109/JQE.2008.924434].
- [6] J. Faist, A. Tredicucci, F. Capasso, C. Sirtori, D. L. Sivco, J. N. Baillargeon, A. L. Hutchinson and A. Y. Cho, "High-power continuous-wave quantum cascade lasers," *IEEE J. Quantum Electron.* **36**, 336-343 (1998) [doi:10.1109/3.658728].
- [7] U. Bockelmann and G. Bastard, "Phonon scattering and energy relaxation in two-, one-, and zero-dimensional electron gases," *Phys. Rev. B* **42**, 8947-8951 (1990) [doi:10.1103/PhysRevB.42.8947].
- [8] H. Benisty, C. M. Sotomayor-Torres, and C. Weisbuch, "Intrinsic mechanism for the poor luminescence properties of quantum-box systems," *Phys. Rev. B* **44**, 10945-10948 (1991) [doi:10.1103/PhysRevB.44.10945].
- [9] R. Heitz, M. Grundmann, N. N. Ledentsov, L. Eckey, M. Veit, D. Bimberg, V. M. Ustinov, A. Yu. Egorov, A. E. Zhukov, P. S. Kope'v, and Zh. I. Alferov,

- "Multiphonon-relaxation processes in self-organized InAs/GaAs quantum dots," *Appl. Phys. Lett.* **68**, 361-363 (1996) [doi:10.1063/1.116716].
- [10] J. Urayama, T. B. Norris, J. Singh, and P. Bhattacharya, "Observation of phonon bottleneck in quantum dot electronic relaxation," *Phys. Rev. Lett.* **86**, 4930-4933 (2001) [doi:10.1103/PhysRevLett.86.4930].
- [11] L. Rebohle, F. F. Schrey, S. Hofer, G. Strasser, and K. Unterrainer, "Energy level engineering in InAs quantum dot nanostructures," *Appl. Phys. Lett.* **81**, 2079-2081 (2002) [doi:10.1063/1.1506419].
- [12] S. Sauvage, P. Boucaud, R. P. S. M. Lobo, F. Bras, G. Fishman, R. Prazeres, F. Glotin, J. M. Ortega, and J.-M. Gérard, "Long polaron lifetime in InAs/GaAs self-assembled quantum dots," *Phys. Rev. Lett.* **88**, 177402 (2002) [doi:10.1103/PhysRevLett.88.177402].
- [13] Z.-K. J. Wu, H. Choi, T. B. Norris, A. Stiff-Roberts, and P. Bhattacharya, "Ultrafast electronic dynamics in unipolar n-doped InAs/GaAs quantum dot structures," in *Conf. Lasers Electro-Optics/Quantum Electron. Laser Sci. Photonic Applications Systems Technol.*, Technical Digest (CD) paper QThC6, OSA/IEEE (2005).
- [14] E. A. Zibik, L. R. Wilson, R. P. Green, G. Bastard, R. Ferreira, P. J. Phillips, D. A. Carder, J.-P. R. Wells, J. W. Cockburn, M. S. Skolnick, M. J. Steer, and M. Hopkinson, "Intraband relaxation via polaron decay in InAs self-assembled quantum dots," *Phys. Rev. B* **70**, 161305(2004) [doi:10.1103/PhysRevB.70.161305].
- [15] B. Kochman, A. D. Stiff-Roberts, S. Chakrabarti, J. D. Phillips, S. Krishna, J. Singh, and P. Bhattacharya, "Absorption, carrier lifetime, and gain in InAs-GaAs quantum-dot infrared photodetectors," *IEEE J. Quantum Electron.* **39**, 459-467 (2003) [doi:10.1109/JQE.2002.808169].
- [16] L. Jacak, J. Krasnyi, D. Jacak, and P. Machnikoski, "Magnetopolaron in a weakly elliptical InAs/GaAs quantum dot," *Phys. Rev. B* **67**, 035303 (2003) [doi:10.1103/PhysRevB.67.035303].
- [17] C.-F. Hsu, J.-S. O, P. Zory, and D. Botez, "Intersubband quantum-box semiconductor lasers," *IEEE J. Sel. Top. Quantum Electron.* **6**, 491-503 (2000) [doi:10.1109/2944.865104].
- [18] I. A. Dmitriev and R. A. Suris, "Quantum cascade lasers based on quantum dot superlattice," *phys. stat. sol. [a]* **202**, 987-991 (2005) [doi:10.1002/pssa.200460714].
- [19] I. C. Sandall, P. M. Smowton, C. L. Walker, H. Y. Liu, M. Hopkinson, and D. J. Mowbray, "Recombination mechanisms in 1.3 μm InAs quantum-dot lasers," *IEEE Photon. Technol. Lett.* **18**, 965-967 (2006) [doi:10.1109/LPT.2006.873560].
- [20] M. D'Souza, D. Xu, J. C. Shin, J. Kirch, L. J. Mawst, D. Botez, I. Vurgaftman, and J. R. Meyer, "Deep-well 4.8 μm -emitting quantum-cascade lasers grown by MOCVD," *21st IEEE Int. Semiconductor Laser Conf.*, paper TuA4, IEEE, CD-ROM (2008).
- [21] N. S. Wingreen and C. A. Stafford, "Quantum-dot cascade laser: proposal for an ultralow-threshold semiconductor laser," *IEEE J. Quantum Electron.* **33**, 1170-1173 (1997) [doi:10.1109/3.594880].
- [22] C.H. Fischer, P. Bhattacharya, and P.-C. Yu, "Intersublevel electroluminescence from $\text{In}_{0.4}\text{Ga}_{0.6}\text{As}/\text{GaAs}$ quantum dots in quantum cascade heterostructure with GaAsN/GaAs superlattice," *Electron. Lett.* **39**, 1537 (2003) [doi:10.1049/el:20030970].
- [23] G. Tsvid, M. D'Souza, D. Botez, B. Hawkins, A. Khandekar, T. Kuech, and P. Zory, "Towards intersubband quantum box lasers: e-beam lithography update," *J. Vac. Sci. Technol. B* **22**, 3214-3216 (2004) [doi:10.1116/1.1824055].
- [24] D. P. Xu, A. Mirabedini, M. D'Souza, S. Li, D. Botez, A. Lyakh, Y.-J. Shen, P. Zory, and C. Gmachl, "Room-temperature, mid-infrared ($\lambda=4.7\mu\text{m}$) electroluminescence from single-stage, intersubband GaAs-based edge emitters," *Appl. Phys. Lett.* **85**, 4573-4575 (2004) [doi:10.1063/1.1819518].

- [25] Y. Bai, S. R. Darvish, S. Slivken, W. Zhang, A. Evans, J. Nguyen, and M. Razeghi, "Room temperature continuous wave operation of quantum cascade lasers with watt-level optical power," *Appl. Phys. Lett.* **92**, 101105 (2008) [doi:10.1063/1.2894569].
- [26] M. A. Reed, J. N. Randall, R. J. Aggarwal, R. J. Matyi, T. M. Moore, and A. E. Wetsel, "Observation of discrete electronic states in a zero-dimensional semiconductor nanostructure," *Phys. Rev. Lett.* **60**, 535-537(1988) [doi:10.1103/PhysRevLett.60.535].
- [27] M. K. Rathi, G. Tsvid, M. D'Souza, J. C. Shin, D. Botez, and T. F. Kuech, "Optimization of fabrication steps for InP-based intersubband quantum boxes (IQBs)," presented at *2008 Electronic Materials Conf.*, June 23-25th 2008, Q2, Minerals, Metals & Materials Soc., Santa Barbara, CA.